J Therm Anal Calorim (2011) 103:925–933
DOI 10.1007/s10973-010-1126-9

Co-firing of biomass with coals

Part 1. Thermogravimetric kinetic analysis of combustion of fir (*abies bornmulleriana*) wood

Ahu Gümrah Dumanli · Sinem Taş · Yuda Yürüm

Received: 16 September 2010 / Accepted: 20 October 2010 / Published online: 4 November 2010

Abstract The chemical composition and reactivity of fir (*Abies bornmulleriana*) wood under non-isothermal thermogravimetric (TG) conditions were studied. Oxidation of the wood sample at temperatures near 600 °C caused the loss of aliphatics from the structure of the wood and created a char heavily containing C–O functionalities and of highly aromatic character. On-line FTIR recordings of the combustion of wood indicated the oxidation of carbonaceous and hydrogen content of the wood and release of some hydrocarbons due to pyrolysis reactions that occurred during combustion of the wood. TG analysis was used to study combustion of fir wood. Non-isothermal TG data were used to evaluate the kinetics of the combustion of this carbonaceous material. The article reports application of Ozawa–Flynn–Wall model to deal with non-isothermal TG data for the evaluation of the activation energy corresponding to the combustion of the fir wood. The average activation energy related to fir wood combustion was 128.9 kJ/mol, and the average reaction order for the combustion of wood was calculated as 0.30.

Keywords Co-firing · Combustion · Thermogravimetric analysis · Non-isothermal kinetics · Activation energy of combustion

Introduction

Biomass (wood, agricultural residues, forestry residues, energy crops, etc.) is a renewable fuel and the fourth largest following coal, oil, and natural gas [1]. Compared with fossil fuels, biomass has the advantages of being harmless in regard to the emissions of carbon dioxide, as this participates in biomass growth through the photosynthesis reactions, and reducing pollutant species generation, given the low sulfur and nitrogen contents. From an economic point of view, the possibility of co-firing of biomass with coal in power plants can be an interesting alternative, since it allows for the use of existing infrastructures already equipped with proper devices for emission control, reducing simultaneously fossil fuels consumption [2]. Information of the chemical composition and reactivity of the biomass, the thermal phenomena occurring during solid fuels combustion is very important for the effective operation of conversion units.

Thermal analysis methods have been extensively used in recent years, because they offer a quick quantitative technique for the assessment of pyrolysis or combustion processes under non-isothermal conditions and allow to guess the effective kinetic parameters for the various decomposition reactions [3–13]. Kinetics of coal-biomass combustion has been investigated by many research groups recently [14–17].

The reaction kinetics parameters of combustion of wood under differential oxidizing conditions were calculated with the method given in Sanchez et al. [18] as follows. The rate of heterogeneous solid-state reactions can generally be explained by

$$\frac{d\alpha}{dt} = k(T)\, f(\alpha) \tag{1}$$

where t is time, $k(T)$ the temperature-dependent constant, and $f(\alpha)$ a function described the reaction model, which expresses the dependence of the reaction rate on the extent of reaction, α. The temperature dependence of the rate

A. G. Dumanli · S. Taş · Y. Yürüm (✉)
Faculty of Engineering and Natural Sciences, Sabanci University, Orhanli, Tuzla, Istanbul 34956, Turkey
e-mail: yyurum@sabanciuniv.edu

constant is explained by the Arrhenius equation. Thus, the rate of a solid-state reaction can generally be illustrated by

$$\frac{d\alpha}{dt} = Ae^{-\frac{E}{RT}} f(\alpha) \quad (2)$$

where A is the pre-exponential Arrhenius factor, E the activation energy, and R the gas constant.

For dynamic data obtained at a constant heating rate

$$\beta = \frac{dT}{dt} = \text{constant}$$

this term is inserted in Eq. 2 so the above rate expression can be converted into non-isothermal rate expressions describing reaction rates as a function of temperature at a constant β.

$$\frac{d\alpha}{dT} = \frac{1}{\beta} Ae^{-\frac{E}{RT}} f(\alpha) \quad (3)$$

Integrating up to conversion, α, Eq. 3 gives,

$$\int_0^{\alpha} \frac{d\alpha}{f(\alpha)} = g(\alpha) = \frac{A}{\beta} \int_{T_0}^{T} e^{-\frac{E}{RT}} dT \quad (4)$$

Isoconversional methods include carrying out a series of experiments at different heating rates [19, 20]. In this study, activation energies from dynamic data were obtained from isoconversional method by Ozawa [21, 22], Flynn and Wall [23] using the Doyle's approximation of $p(x)$ [24], which involves measuring the temperatures corresponding to fixed values of α from experiments at different heating rates.

$$\ln(\beta) = \ln\left[\frac{AE}{Rg(\alpha)}\right] - 5331 - 1052\,\frac{E}{RT} \quad (5)$$

From this equation, the activation energy E may be estimated by plotting ln (β) versus $1/T$.

To find out the reaction order, Avrami's theory [25–27] was used to describe non-isothermal cases, where variation of the degree of conversion with temperature and heating rate can be explained as

$$\alpha(T) = 1 - \exp\left[-\frac{k(T)}{\beta^n}\right] \quad (6)$$

Taking the double natural logarithm of both sides of Eq. 6, with $k(T) = Ae^{-E/RT}$, yields

$$\ln[-\ln(1-\alpha(T)] = \ln A - \frac{E}{RT} - n\ln\beta \quad (7)$$

Therefore, a plot of $\ln[-\ln(1-\alpha(T)]$ versus $\ln\beta$, which is obtained at the same temperature from a number of isotherms taken at different heating rates, should give in straight lines whose slope will have the value of the reaction order or the Flynn–Wall–Ozawa exponent n [21, 28]. Extra aspects of the technique applied to examine the process are explained by Ozawa [22].

The aim of this study was to determine the chemical composition and reactivity of fir wood under non-isothermal thermogravimetric (TG) conditions. This study provided a kinetic evaluation of the combustion of fir wood. The Ozawa–Flynn–Wall model was used to deal with non-isothermal TG data to calculate the activation energy of the fir wood combustion. The data obtained will be useful to understand the behavior of fir wood during combustion. The information obtained will be used in the co-firing of the wood with low rank Turkish coals.

Experimental

Materials and characterization

The fir wood sample used in this study was a bark-free fir (*Abies bornmulleriana*) sawdust sample obtained from Bolu forests (northwest Anatolia) in Turkey. The proximate and elemental analyses of the wood sample were done at the Instrumental Analysis Laboratory of the Scientific and Technical Research Council of Turkey, Ankara, is given in Table 1. The sawdust was ground and sieved to below 175 μm (−80 mesh) size. Wood sample was characterized in terms of proximate analysis according to the ASTM standards (ASTM E871, ASTM D1102-84, ASTM D3172-89) using laboratory furnaces, ultimate analysis using CHN-600 and S532-500 analyzers (ASTM D3176-93, ASTM D3177-33). Calorific values of the samples were determined with a Parr 6100 calorimeter according to ASTM D2015-95 in our laboratories.

Thermogravimetric analysis

Wood combustion tests were performed in a Netzsch STA 449 C Jupiter differential thermogravimetric analyzer (precision of temperature measurement ±2 °C, microbalance sensitivity <5 μg), with which the sample weight loss

Table 1 Proximate and elemental analyses of fir wood

Proximate analysis/% (as received)	
Volatile matter	85.5
Fixed carbon	10.5
Moisture	3.7
Ash	0.3
Elemental analysis/% (daf)	
Carbon	47.2
Hydrogen	6.1
Nitrogen	0.3
Oxygen (by difference)	46.7
H/C (atomic)	1.55

and rate of weight loss as functions of time or temperature were recorded continuously, under dynamic conditions, in the range 25–1000 °C. The experiments were carried out under an air atmosphere, with a flow rate of 60 mL/min, and combustion of the samples was performed in the furnace of the thermobalance under controlled temperature to obtain the corresponding TG curves with heating rates (β) of 5, 10, 20, and 30 °C/min as it was also conducted in current literature [29, 30]. Preliminary tests with different sample masses and sizes and gas flow rates were carried out, to check the influence of heat and mass transfer. 20–25 mg of each material, of −250 μm particle size, was found to be optimum to eliminate the effects of eventual side reactions and mass and heat transfer limitations, was thinly distributed in the crucible in the experiments. The experiments were replicated at least twice to determine their reproducibility, which was found to be satisfactory.

The TG–FTIR runs were carried out in a Netzsch STA 449 C Jupiter TG system coupled to a Bruker Equinox 55 FTIR spectrometer under a dynamic air atmosphere. TG analysis was done from 25 to 1000 °C at a linear heating rate of 10 °C/min. The output of the TGA system was connected to the FTIR spectrometer through a heated line. The balance adapter, the transfer line, and the FTIR gas cell can be heated until 250 °C, thus avoiding the condensation of the less volatile compounds. On the other hand, the low volumes in the thermobalance microfurnace, transfer line, and gas measurement cell permit low carrier gas flow rates to be used and allow for good detection of the gases evolved in the pyrolysis process. In all the experiments, the transfer line and the gas measurement cell were maintained at 200 °C. Online gas analyses were performed for the detection of combustion gases fed to FTIR spectrometer, and experimental data were stored as a function of time.

FTIR spectra

FTIR spectra of the original and fir wood samples oxidized under an air atmosphere at 200, 300, 350, 380, 400, 500, and 600 °C were obtained using a Bruker Equinox 55 FTIR spectrometer equipped with an ATR system by co-adding 20 scans over the range 600–4000 cm^{-1} performed at 1 cm^{-1} of digital resolution. The assignment of the bands in the FTIR spectra was according to Shevla [31].

Scanning electron microscopy

Morphology of the wood and its ashes was examined by scanning electron microscopy. Leo Supra 35VP Field emission scanning electron microscope (SEM), Leo 32 and energy dispersive X-ray spectrometer (EDS) were used for images and analyses of the major ash-forming elements in different ashes. Wood and ash samples were mounted on stubs and gold-coated before analysis, to make them electrically conductive. Imaging was generally done at 2–5 keV accelerating voltage, using the secondary electron imaging technique.

Results and discussion

SEM–EDS analysis

Morphology of the wood and its ash obtained at 900 °C was investigated by SEM, Fig. 1. Physical appearances of wood and its ashes were quite different. The SEM photographs indicated that these contained material with diverse morphology. While micro structure of the wood contained amorphous, the ash was consisted of some prismatic, mainly micron-scale cubical forms of 0.2 μm size. EDS analysis of the wood ash revealed, Table 2, that the ash contained unburned carbon and in the order of decreasing percentage oxides of calcium, aluminum, potassium, magnesium, and sodium. Ash elements can exert a catalytic role on the reactivity of organic material during combustion of the wood. Karabakan and Yürüm [32] found that mainly carbonates of calcium and magnesium have a mild

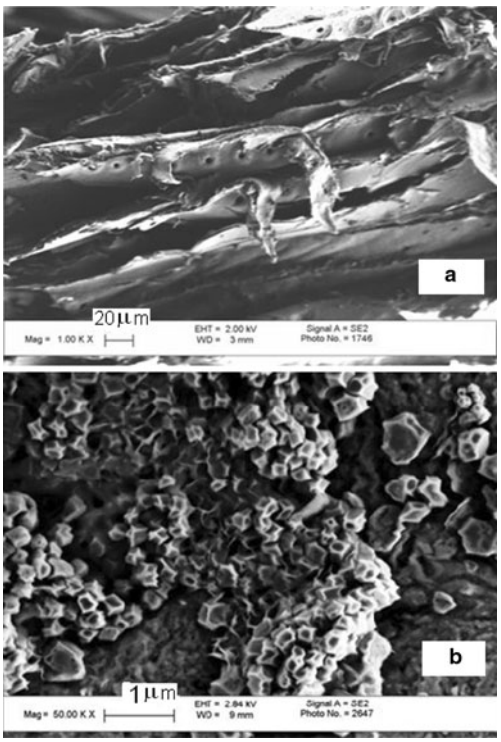

Fig. 1 SEM micrographs of **a** fir wood and **b** residue of fir wood fired at 900 °C

Table 2 EDS analysis results of the ash obtained at 900 °C

Element	Series	Net	Unnor. wt%	Norm. wt%	At.%
Carbon	K series	293	5.9456	5.2861	10.3084
Oxygen	K series	2458	39.9036	35.4771	51.9369
Magnesium	K series	164	1.2457	1.1075	1.0673
Calcium	K series	305	43.7126	38. 8635	22.7127
Sodium	K series	76	0.5506	0.4895	0.4987
Aluminum	K series	1035	9.3138	8.2806	7.1883
Potassium	K series	197	11.8048	10.4953	6.2874

effect to promote the oxidation organic material in carbonaceous fuels.

FTIR analysis of the original and oxidized fir wood

FTIR spectra recorded in the 400–4000 cm^{-1} region of original fir wood and oxidized fir wood are presented in Fig. 2. FTIR spectrum of the wood, Fig. 2a, contained a strong broad O–H stretching at 3300–4000 cm^{-1}, C–H stretching at 2800–3000 cm^{-1}, and several distinct peaks in the finger print region between 500 and 1750 cm^{-1}. Most of these bands have contribution from both carbohydrates (cellulose and hemicellulose) and lignin. More specifically, the bands at 3431 and 1450 cm^{-1} (characteristic of hydrogen bonded OH groups), 2927 and 1470 cm^{-1} (C–H stretching of methyl or methylene groups) [31]. The band at 1738 cm^{-1} in the spectrum of the wood is due to uranic acid and acetyl groups in the hemicellulosic material of the wood [33]. The presence of a sharp signal at 1643 cm^{-1} can be attributed to the aromatic rings in quinonic structures. Specific band maxima in 1260–1000 cm^{-1} regions were related with ring vibrations overlapped with stretching vibrations of (C–OH) side groups and the (C–O–C) glycosidic bond vibration, typical of xylans. Bands at 1267 and 1057 cm^{-1} are indicative of hemicelluloses. Bands in the range of 1270–1050 cm^{-1} belong to C–O and C–O–C groups [33].

The FTIR spectra of the wood oxidized at 200, 300, 350, 380, 400, 500, and 600 °C are presented between Fig. 2b and h, respectively. The significant change in the spectra of

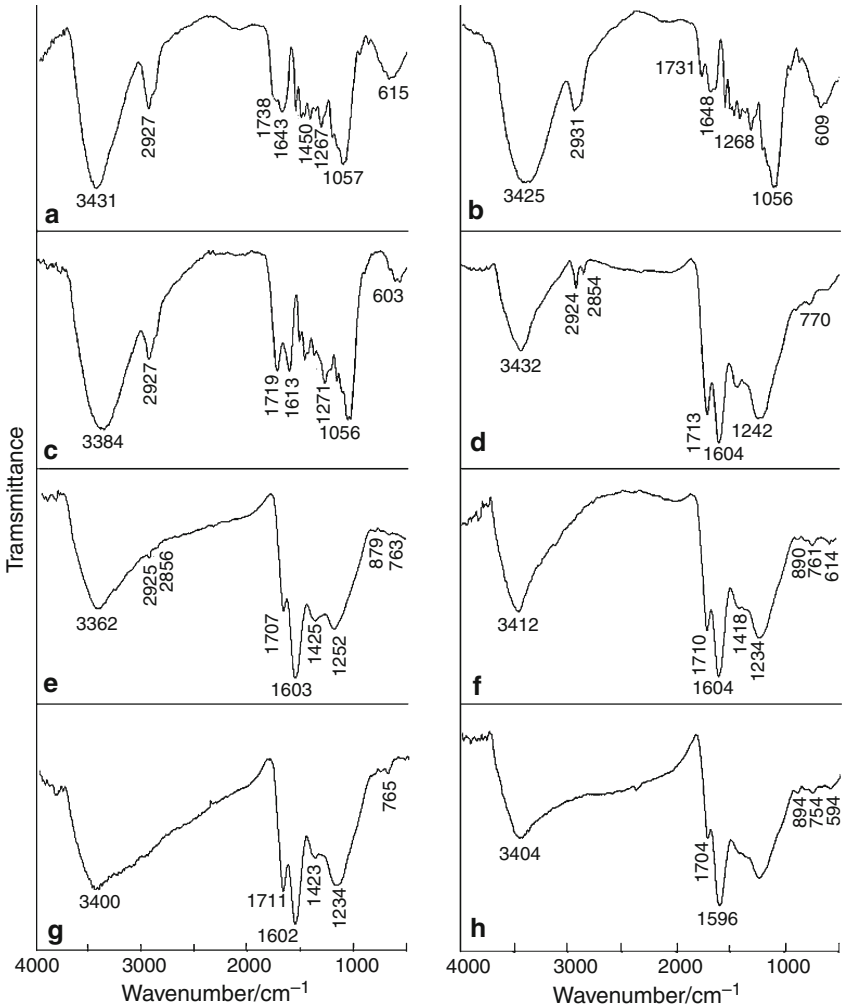

Fig. 2 FTIR spectra of **a** original fir wood and fir wood oxidized at **b** 200 °C, **c** 300 °C, **d** 350 °C, **e** 380 °C, **f** 400 °C, **g** 500 °C, and **h** 600 °C

oxidized wood seemed in the intensity of C–H stretching of methyl or methylene peaks in the zone 2930–2924 cm^{-1}, decreased steadily until 380 °C and beyond this temperature these functionalities appeared to be lost. The other significant change was the nascence of new absorption bands due to oxygenated functions such as C–O distinguished in the zone of 1731 and 1704 cm^{-1}. As the oxidation temperature was increased from 300 to 600 °C intensity of the C–O band increased and the peaks shifted from 1731 to 1704 cm^{-1} strongly suggesting a rearrangement among the C–O functionalities during oxidation, the 1734 cm^{-1} band is characteristic of non-conjugated carbonyl group [34]. The third important change was sharp increase in the intensity of the absorption bands due to aromatic ring breathing vibrations near 1600 cm^{-1}, indicating the formation of a product of high aromaticity. Therefore, oxidation of the wood sample at temperatures near 600 °C caused the loss of aliphatics from the structure of the wood and created a char heavily containing C–O functionalities and of highly aromatic character.

TG–FTIR experiments

The evolution of gaseous species and products as a result of the oxidation of wood sample was simultaneously monitored by FTIR during the TG experiment at the heating rate of 10 °C/min. The FTIR spectra of the gases evolved during are presented in Fig. 3. The spectra were detected at increasing times, and the corresponding temperatures at which the spectra were recorded are denoted on the spectra. Spectra indicated the nascence and development of certain peaks. Bernstein et al. [35] who investigated the infrared spectra of CO_2 indicated the following peaks were due to CO_2: 3720, 3600, 3300, 2375, 1620, 750, and 675 cm^{-1}. Lemus [36] who studied on infrared spectra of water vapor showed that the peaks at 3756, 3657, and 1594 cm^{-1} were due to water vapor. Spectra recorded in this study contained the following peaks: 3720, 3563, 2375, and 1688 cm^{-1} due to CO_2, 3188 [37] and 1550 cm^{-1} due to water vapor, and 844 cm^{-1} due to hydrocarbons. The large peak at 3188 cm^{-1} in the spectrum obtained in the 2833rd second that was due to water vapor indicated the combustion of hydrogen content of the wood, that was also an indication of high hydrogen content of the wood (H/C = 1.55). On-line FTIR recordings of the combustion of wood indicated the oxidation of carbonaceous and hydrogen content of the wood and release of some hydrocarbons due to pyrolysis reactions that occurred during combustion of the wood.

Heat treatment of wood under oxidative and non-oxidative atmospheres

In this study, the wood sample was subjected to heat treatment at different temperatures between 100 and 400 °C in the presence of air. The mass loss according to the heat treatment was recorded, and calorific values of the samples were measured using an adiabatic calorimeter. The results were compared with the untreated wood sample. Results are shown in Table 3. According to the calorific value results, during the heat treatment of the wood sample under an air atmosphere, up to 200 °C the calorific value of the wood increased from 18746 to 19521 kJ/kg due to the removal of the low volatile compounds. As the heat treatment temperature was increased to 300 °C and higher temperatures, parallel to the pyrolytic losses of carbonaceous material from the structure of the wood and combustion of the carbonaceous material the calorific values decreased sharply to 3149 kJ/kg.

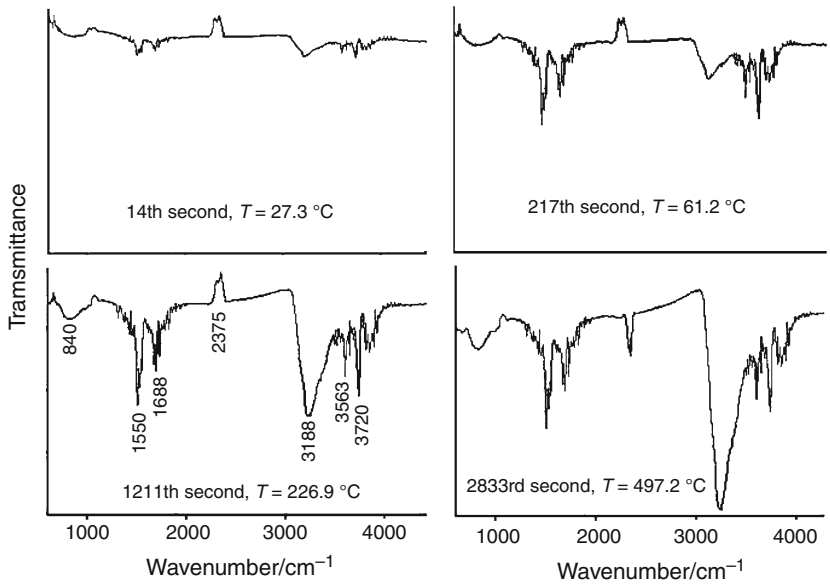

Fig. 3 TGA–FTIR spectra of gases released during combustion of fir wood heated under a dynamic air atmosphere from 25 to 1000 °C by a heating rate of 10 °C/min

Table 3 Effect of heat treatment under an air atmosphere on the calorific values of the wood

Heat treatment temperature/°C	Mass loss/%	Calorific value/kJ/kg
Unheated	–	18746
100	5.9	19135
200	11.0	19521
300	32.0	3149
400	99.3	–

Table 4 Effect of heat treatment under an argon atmosphere on the calorific values of the wood

Heat treatment temperature/°C	Mass loss/%	Calorific value/kJ/kg
Unheated	–	18746
100	10.1	19001
200	11.7	19910
300	27.0	24210
400	97.1	–

The same experiment was repeated under an argon atmosphere, and the results are shown in Table 4. In these experiments, the calorific values steadily increased from 18746 to 24210 kJ/kg due to the removal of volatiles producing residual matter rich in carbon. Further increase of the temperature volatilized all the carbonaceous material. The TG experiments gave information of the percent material loss during heat treatment.

TG experiments

This study on reactivity of wood, useful for kinetic analysis, was mainly based on TG measurements. DTG tracings obtained during the oxidation of wood with different heating rates were presented in Fig. 4. The TG curves measured from the temperature programmed combustion of the wood samples at the heating rates (β) of 5, 10, 20, and 30 °C/min were illustrated in Fig. 5. As it might be examined, on raising the temperature, combustion of the sample occurred with a related mass loss. Once the fuel content of the wood was consumed, the mass corresponding to the ashes stayed constant. Given the small sample amounts and the relatively slow heating rates, the weight loss versus temperature curves showed several sequential zones, as in the example for wood exposed to air. The weight loss versus temperature curves showed several sequential zones, as in the example for wood exposed to air. The first zone of weight loss, temperatures below 390 °C and conversion up to 60%, was the pyrolysis (or devolatilization) stage, whose characteristics were affected

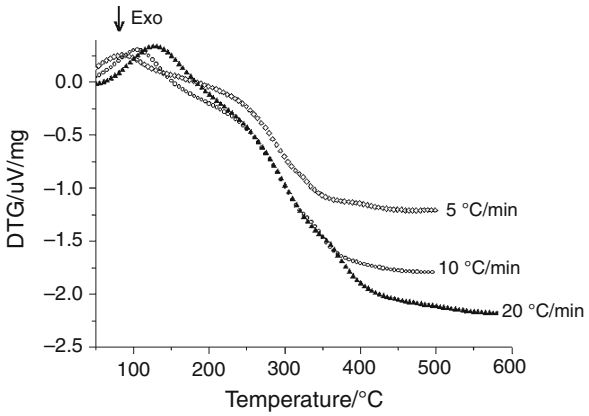

Fig. 4 DTG tracings obtained during the oxidation of wood with different heating rates

by the presence of oxygen in the reaction environment. Char oxidation, adjoining solid pyrolysis, was completed at about 875 °C.

Figure 5 shows the TG mass loss curve of the wood with at various heating rates (β) (5, 10, 20, and 30 K/min) to study the effect of heating rate on non-isothermal kinetics. There were two main temperatures for mass losses for every heating rate (Fig. 5). The first temperature range was 339.2–381.1 °C; as the heating rate was increased the greater mass losses were detected at higher temperatures. The second temperature range at which more material loss occurred was 537.9–875.7 °C; in this range, higher heating rates caused higher losses at more elevated temperatures. Residual masses in the range of 1.01–2.24% were obtained at about 1009–1019 °C. So there were several steps for mass losses; at 95 °C humidity of the wood was lost, depending on the heating rate at about 340–380 °C, 56–62% of the volatiles were lost and in the temperature range of 540–875 °C the total material loss reached to 96–98%. Higher heating rates caused higher material loss compared to the loss of material at lower heating rates. Since small masses of wood (20–25 mg) were utilized in each experiment, and particle size of the wood was reduced to <250 μm, mass and heat transfer limitations were eliminated. The data obtained using different heating rates during firing experiments, therefore, did not contain any restrictive resistances. As the heating rate was increased, the maximum mass loss and/or maximum rate of combustion shifted to higher temperatures. This was attributed to the changes in the rate of heat transfer with the increase in the heating rate and the short exposure time to a particular temperature at high heating rates, as well as the effect of the kinetics of combustion.

Eight different percentages of conversion (α) are pointed out in each curve in Fig. 5: 10, 10, 20, 30, 40, 50, 70, 80, and 90%. The plots of ln β versus $1/T$ corresponding to the several conversion degrees of the process were shown in

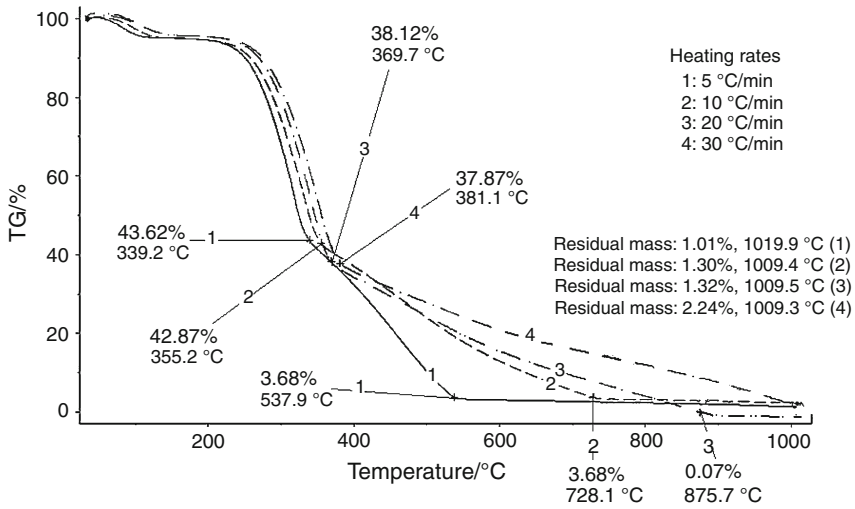

Fig. 5 TG tracings obtained during the oxidation of wood with different heating rates in the temperature range of 25–1000 °C

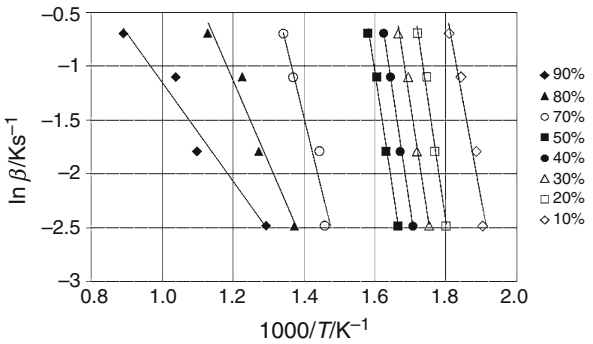

Fig. 6 Curves of fitting to kinetic model proposed by Ozawa–Flynn–Wall to various conversion percentages corresponding to the combustion of fir wood at different heating rates for the calculation of activation energies

Fig. 6 for wood. Generally, there were linear relations for the conversion percentages so the activation energies were calculated from the corresponding slopes according to the Ozawa–Flynn–Wall kinetic method, Table 5. Raising the temperature, combustion of the sample occurred with mass losses and related decrease in activation energies. Activation energy calculated at 10% conversion was 142.3 kJ/mol and steadily increased until 50% conversion to a value of 169.8 kJ/mol then as the material loss increased beyond this point, the activation energy started to decrease until to 36.4 kJ/mol at conversion of 90%. It seemed that the first phase of reactions constituted the rate determining set of reactions with average activation energy of 165.8 kJ/mol. Beyond 70% conversion in combustion reactions, the average activation energy dropped to 67.6 kJ/mol. The overall average activation energy of the combustion of the wood was calculated to be 128.9 kJ/mol. This value calculated for fir wood seemed to be higher than those, 54–92 kJ/mol, calculated by Kök [38] for some Turkish low rank coals using Coats and Redfern method [39], but lower than those calculated for the combustion of biomass using the Ozawa–Flynn–Wall kinetic method, 140 kJ/mol [18]. Otero et al. [40] using the Ozawa–Flynn–Wall kinetic method with a semianthracite coal calculated the average activation energy of combustion as 67.3 kJ/mol.

Table 5 Slopes and correlation coefficients (R^2) corresponding to linear fittings to kinetic model proposed by Ozawa–Flynn–Wall to various conversion percentages corresponding to the combustion of wood at different heating rates together with the resultant activation energy (E) values

Conversion/%	R^2	Slope	Activation energy/kJ/mol	Average activation energy/kJ/mol
10	0.953	−18.01	142.3	Rate determining phase 165.8
20	0.987	−22.51	177.9	
30	0.988	−21.07	166.5	
40	0.997	−21.83	172.5	
50	0.993	−21.48	169.8	
70	0.936	−13.44	106.2	Fast reactions 67.6
80	0.959	−7.61	60.1	
90	0.951	−4.61	36.4	
Overall average activation energy/kJ/mol				128.9

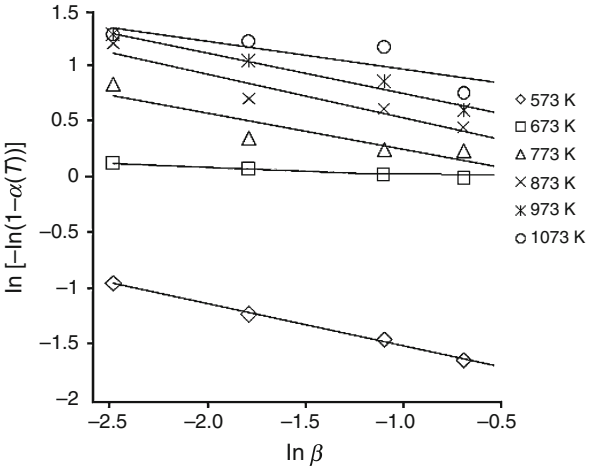

Fig. 7 Straight lines fitting to Ozawa–Flynn–Wall kinetic model for various conversion percentages corresponding to the combustion of wood at different heating rates for the determination of reaction order *n*

Table 6 Reaction order (*n*) as a function of temperature for the combustion of wood

T/°C	Reaction order/*n*
300	0.38
400	0.10
500	0.32
600	0.39
700	0.36
800	0.25
Average *n*	0.30

For the computation of the reaction order, the plots of $\ln[-\ln(1-\alpha(T)]$ versus $\ln \beta$ have been represented in Fig. 7. The *n* values as a function of temperature for wood combustion are shown in Table 6. The values changed from very close to zero to around 0.3 and are dependent on the extent of the reaction, i.e., not constant during the reaction, which was an evidence of the multiple step processes such as devolatilization and combustion. The lowest value for *n* was measured at 400 °C at which the slope of the % TG versus temperature curves changed sharply indicating a change in the combustion regime. After this temperature, the order of the reaction again raised to values close to the average value of 0.30.

Conclusions

EDS analysis of the wood ash revealed that the ash contained unburned carbon and in the order of decreasing percentage oxides of calcium, aluminum, potassium, magnesium, and sodium. Oxidation of the wood sample at temperatures near 600 °C caused the loss of aliphatics from the structure of the wood and created a char heavily containing C–O functionalities and of highly aromatic character. On-line FTIR recordings of the combustion of wood indicated the oxidation of carbonaceous and hydrogen content of the wood and release of some hydrocarbons due to pyrolysis reactions that occurred during combustion of the wood. Heat treatment of the wood sample under an air atmosphere, up to 200 °C, caused the calorific value of the wood to increase from 18746 to 19521 kJ/kg due to the removal of the low volatile compounds. As the heat treatment temperature was increased to 300 °C and higher temperatures, parallel to the pyrolytic losses of carbonaceous material from the structure of the wood and combustion of the carbonaceous material the calorific values decreased sharply to 3149 kJ/kg. The weight loss versus temperature curves showed several sequential zones, as in the example for wood exposed to air. The first zone of weight loss, temperatures below 390 °C and conversion up to 60%, was the pyrolysis (or devolatilization) stage, whose characteristics were affected by the presence of oxygen in the reaction environment. Char oxidation, adjoining solid pyrolysis, was completed at about 875 °C. It seemed that the first phase of reactions constituted the rate determining set of reactions with average activation energy of 165.8 kJ/mol. Beyond 70% conversion in combustion reactions, the average activation energy dropped to 67.6 kJ/mol. The overall average activation energy of the combustion of the wood was calculated to be 128.9 kJ/mol. The value of order of reaction changed from very close to zero to around 0.3 and are dependent on the extent of the reaction, i.e., not constant during the reaction, which was an evidence of the multiple step processes.

References

1. Di Blasi C. Combustion and gasification rates of lignocellulosic chars. Progress Energ Comb Sci. 2009;35:121–40.
2. Vamvuka D, Salpigidou N, Kastanaki E, Sfakiotakis S. Possibility of using paper sludge in co-firing applications. Fuel. 2009; 88:637–43.
3. Várhegyi G, Szabó P, Jakab E, Till F. Mathematical modeling of char reactivity in Ar-O_2 and CO_2–O_2 mixtures. Energ Fuels. 1996;10:1208–14.
4. Ceylan K, Karaca H, Önal Y. Thermogravimetric analysis of pretreated Turkish lignites. Fuel. 1999;78:1109–16.
5. Adánez J, De Diego LF, García-Labiano F, Abad A, Abanades JC. Determination of biomass char combustion reactivities for fbc applications by a combined method. Ind Eng Chem Res. 2001;40:4317–23.
6. Otero M, Díez C, Calvo LF, García AI, Mordu A. Analysis of the co-combustion of sewage sludge and coal by TG-MS. Biomass Bioenerg. 2002;22:319–29.

7. Quanrum L, Haoquan H, Qiang Z, Shengwei Z, Gouohua C. Effect of inorganic matter on reactivity and kinetics of coal pyrolysis. Fuel. 2004;83:713–8.
8. Mianowski A, Bigda R, Zymla V. Study on kinetics of combustion of brick-shaped carbonaceous materials. J Therm Anal Calorim. 2006;84:563–74.
9. Franceschi E, Cascone I, Nole D. Thermal, XRD and spectrophotometric study on artificially degraded woods. J Therm Anal Calorim. 2008;91:119–25.
10. Xu Q, Griffin GJ, Jiang Y, Preston C, Bicknell AD GP, Bradbury GP, White N. Study of burning behavior of small scale wood crib with cone calorimeter. J Therm Anal Calorim. 2008;91:787–90.
11. Yu LJ, Wang S, Jiang XM, Wang N, Zhang CQ. Thermal analysis studies on combustion characteristics of seaweed. J Therm Anal Calorim. 2008;93:611–7.
12. Otero M, Gómez X, García AI, Morán A. Non-isothermal thermogravimetric analysis of the combustion of two different carbonaceous materials coal and sewage sludge. J Therm Anal Calorim. 2008;93:619–26.
13. Suarez AC, Tancredi N, Cesar P, Pinheiro C, Yoshida MI. Thermal analysis of the combustion of charcoals from Eucalyptus dunnii obtained at different pyrolysis temperatures. J Therm Anal Calorim. 2010;100:1051–4.
14. Kastanaki E, Vamvuka D. A comparative reactivity and kinetic study on the combustion of coal–biomass char blends. Fuel. 2006;85:1186–93.
15. Gil MV, Casal D, Pevida C, Pis JJ, Rubiera F. Thermal behaviour and kinetics of coal/biomass blends during co-combustion. Bioresour Technol. 2010;101:5601–8.
16. Muthuraman M, Namioka T, Yoshikawa K. Characteristics of co-combustion and kinetic study on hydrothermally treated municipal solid waste with different rank coals: A thermogravimetric analysis. Appl Energ. 2010;87:141–8.
17. Sahu SG, Sarkar P, Chakraborty N, Adak AK. Thermogravimetric assessment of combustion characteristics of blends of a coal with different biomass chars. Fuel Process Technol. 2010; 91:369–78.
18. Sanchez ME, Otero M, Gomez X, Moran A. Thermogravimetric kinetic analysis of the combustion of biowastes. Renew Energ. 2009;34:1622–7.
19. Vyazovkin S. Evaluation of activation energy of thermally stimulated solid-state reactions under arbitrary variation of temperature. J Comput Chem. 1997;18:393–402.
20. Khawam A, Flanagan DR. Role of isoconversional methods in varying activation energies of solid-state kinetics: II. Nonisothermal kinetic studies. Thermochim Acta. 2005;436:101–12.
21. Ozawa T. A new method of analyzing thermogravimetric data. Bull Chem Soc Jpn. 1965;38:1881–6.
22. Ozawa T. Kinetic analysis of derivative curves in thermal analysis. Therm Anal. 1970;2:301–24.
23. Flynn JH, Wall LA. Structures and thermal analysis of 1,1,6,6-tetraphenylhexa-2,4-diyne-1,6-diol. Polym Lett. 1966;4:323–8.
24. Doyle CD. Estimating isothermal life from thermogravimetric data. J Appl Polym Sci. 1962;6:639–42.
25. Avrami MJ. Kinetics of phase change. I. General theory. Chem Phys. 1939;7:1103–12.
26. Avrami MJ. Kinetics of phase change. II. Transformation-time relations for random distribution of nuclei. Chem Phys. 1940;8: 212–24.
27. Avrami MJ. Kinetics of phase change. III. Granulation, phase change, and microstructure. Chem Phys. 1941;9:177–84.
28. Flynn JH, Wall LA. A general treatment of the thermogravimetry of polymers. J Res Natl Bur Stand. 1966;70A:487–523.
29. Yanfen L, Xiaoqian M. Thermogravimetric analysis of the co-combustion of coal and paper mill sludge. Appl Energ. 2010; 87:3526–32.
30. Di Nola G, de Jong W, Spliethoff H. TG-FTIR characterization of coal and biomass single fuels and blends under slow heating rate conditions: partitioning of the fuel-bound nitrogen. Fuel Process Technol. 2010;91:103–15.
31. Shevla G. Comprehensive analytical chemistry. In: Shevla G, editor. Analytical infrared spectroscopy, vol. VI. Amsterdam: Elsevier; 1976. pp. 334.
32. Karabakan A, Yürüm Y. Effect of the mineral matrix in the reactions of shales. 2. Oxidation reactions of Turkish Göynük and U.S. Western Reference shales. Fuel. 2000;79:785–92.
33. Pakdel H, Grandmaison JL, Roy C. Analysis of wood vacuum pyrolysis solid residues by diffuse reflectance infrared Fourier transform spectroscopy. Can J Chem. 1989;67:310–4.
34. Pandey KK. Study of the effect of photo-irradiation on the surface chemistry of wood. Polym Degrad Stab. 2005;90:9–20.
35. Bernstein MP, Cruikshank DP, Sandford SA. Near-infrared laboratory spectra of solid H_2O/CO_2 and CH_3OH/CO_2 ice mixtures. Icarus. 2005;179:527–34.
36. Lemus R. Vibrational excitations in H_2O in the framework of a local model. J Mol Spectrosc. 2004;225:73–92.
37. Wu Y-W, Sun S-Q, Zhou Q, Tao J-X, Noda I. Volatility-dependent 2D IR correlation analysis of traditional Chinese medicine 'Red Flower Oil' preparation from different manufacturers. J Mol Struct. 2008;882:107–15.
38. Kök MV. Temperature-controlled combustion and kinetics of different rank coal samples. J Therm Anal Calorim. 2005;79: 175–80.
39. Coats AW, Redfern JP. Kinetics parameters from thermogravimetric data. Nature. 1964;201:68–9.
40. Otero M, Calvo LF, Gil MV, Garcia AI, Moran A. Co-combustion of different sewage sludge and coal: a non-isothermal thermogravimetric kinetic analysis. Bioresour Technol. 2008;99: 6311–9.